Experimental characterisation of a CuAg alloy for thermo-mechanical applications. Part 1: Identifying parameters of non-linear plasticity models

Journal:	*Fatigue & Fracture of Engineering Materials & Structures*
Manuscript ID	FFEMS-7100.R1
Manuscript Type:	Original Contribution
Date Submitted by the Author:	n/a
Complete List of Authors:	Benasciutti, Denis; Università di Ferrara, Department of Engineering Srnec Novak, Jelena; Università di Udine, Dipartimento Politecnico di Ingegneria e Architettura Moro, Luciano; Università di Udine, Dipartimento Politecnico di Ingegneria e Architettura De Bona, Francesco; Università di Udine, Dipartimento Politecnico di Ingegneria e Architettura Stanojević, Aleksandar; Montanuniversitat Leoben, Chair of Mechanical Engineering
Keywords:	Cyclic plasticity, kinematic model, isotropic model, parameter identification

Experimental characterisation of a CuAg alloy for thermo-mechanical applications. Part 1: Identifying parameters of non-linear plasticity models

D. Benasciutti[1a], J. Srnec Novak[2], L. Moro[2], F. De Bona[2], A. Stanojević[3]

[1] Department of Engineering, University of Ferrara, via Saragat 1, 44122, Ferrara, Italy

[2] Politechnic Department of Engineering and Architecture (DPIA), University of Udine, via delle Scienze 208, Udine 33100, Italy

[3] Chair of Mechanical Engineering, Montanuniversität Leoben, Franz Josef-Straße 18, Leoben 8700, Austria

Abstract. Despite the wide use of copper alloys in thermo-mechanical applications, there is little data on their cyclic plasticity behaviour, particularly for CuAg alloys. This prevents the behaviour of the materials from being correctly described in numerical simulations for design purposes. In this work CuAg0.1 alloy used for thermo-mechanical applications was tested by strain-controlled cyclic loading at three different temperatures (room temperature, 250 °C, 300 °C). In each test, stress-strain cycles were recorded until the alloy had completely stabilised. These cycles were then used to identify material parameters of non-linear kinematic and isotropic models. The focus was on plasticity models (Armstrong-Frederick, Chaboche, Voce) that are usually implemented in commercial finite element codes. Simulated cyclic responses with the identified material models were compared with experiments, and showed a good agreement. The identified material parameters for the CuAg alloy under investigation can be used directly in finite element models for cyclic plasticity simulations, thus enabling a durability analysis of components under thermo-mechanical loads to be performed, particularly in the field of steel-making plants.

Keywords

cyclic plasticity; kinematic and isotropic model; parameter identification.

[a] Corresponding author.
E-mail: denis.benasciutti@unife.it
Phone: +39 0532 974976
Fax: +39 0532 974870

Nomenclature

b	speed of stabilisation
C	initial hardening modulus
E	elastic modulus
E_1	elastic modulus (at the first cycle)
E_s	elastic modulus (at the stabilised cycle)
N	number of cycles
R	drag stress
R_∞	saturated value of drag stress
$\boldsymbol{S}$	deviatoric stress tensor
$\boldsymbol{X}$	back stress tensor
γ	non-linear recovery parameter
ε_{el}, ε_{pl}, ε_{tot}	strain (elastic, plastic, total)
$\varepsilon_{pl,acc}$	accumulated plastic strain
ε_a	strain amplitude
$\Delta\varepsilon=2\varepsilon_a$	strain range
σ	stress
σ_{y0}	initial yield stress
σ_{yc}	cyclic yield stress
σ_a	stress amplitude
$\sigma_{max,1}$, $\sigma_{max,s}$	maximum stress (at the first and stabilised cycle)
RT	room temperature

1. Introduction

Copper alloys have considerable thermal conductivity and relatively good mechanical properties, thus making them suitable for structures subjected to high thermal flux and mechanical loads.[1] A typical example in the steel-making industry is a mould (also known as a crystallizer), which is a long vertical "tube" positioned at the beginning of a continuous casting line and filled with liquid steel. A mould is usually made of CuAg, CuCrZr or, less frequently, CuNiBe copper alloys.[1] The mould is water cooled to extract sufficient heat to solidify a thin solid shell in the molten steel flowing inside it.

Owing to the vast amount of heat removed, the inner surface of the mould is subjected to high temperatures that cause localised plasticity. Temperatures also fluctuate due to small oscillations in the free surface of liquid steel, as well as due to the periodic plant switch off. These temperature changes cause a cyclic plasticity in critical regions of the mould (typically at the inner surface close to the liquid free surface), where a network of cracks may appear and even propagate through the mould.

As a design requirement, a mould needs to survive several months before being replaced, tolerating a small amount of wear and only non-propagating cracks on its inner surface. In fact, the mould must be completely protected from any through-thickness crack that would bring the molten steel in direct contact with the cooling water, with obvious catastrophic consequences.

Several studies have successfully applied the finite element method for simulating the thermo-mechanical response of the mould under thermal loads. The simulated elasto-plastic stress-strain cycles in critical regions have also been compared to experimental fatigue curves, to estimate crack initiation/propagation and mould service life.[2]

A critical step in finite element modelling is the choice of the material model to simulate cyclic plasticity. Over the last few decades, several plasticity theories have been proposed. Kinematic hardening can be modelled by adopting linear (Prager) or nonlinear (Armstrong & Frederick, Chaboche etc.) models, while cyclic hardening/softening behaviour can be captured with a nonlinear isotropic model (Voce).[3-7] Most theories are now implemented in commercial finite element software and used routinely.[8-11]

The primary criterion for selecting a material model is its ability to represent the experimental material behaviour as closely as possible. Equally important is the possibility to identify material parameters from experiments, or at least to obtain them from the literature.

Parameters of plasticity models are often difficult to find in the literature, and for certain classes of materials, they are not available at all. One example of great interest in continuous-casting plant design, are moulds, which are generally made with CuAg and CuCrZr alloys. While thermo-physical, mechanical and fatigue properties have been collected for the CuCrZr type,[1] little attention has been paid to the CuAg alloy, preventing the finite element modelling of the mould behaviour from being correctly carried out.

This work presents the results of experimental cyclic strain-controlled tests on a CuAg alloy used for continuous-casting moulds. Tests were carried out at three different and constant temperatures (room temperature at 20 °C, 250 °C, 300 °C). These temperatures typically occur in the inner surface of CuAg moulds when they are in service. Stress-strain cycles recorded during tests provide the database for identifying material parameters of non-linear kinematic and isotropic plasticity models.

Simulated cyclic material responses using the set of identified parameters are compared to experimental cyclic data to confirm the ability of the considered plasticity models to adequately represent the elasto-plastic cyclic behaviour of the CuAg alloy under study. As a final result, the set of identified parameters can be directly used in finite element models aimed at simulating the elasto-plastic cyclic response of continuous-casting moulds, whose durability analysis is of great interest for the steel-making industry.

Although this work focuses on the material characterization of a copper alloy for a mould, the proposed procedure can be also extended to other applications and materials: for example, a similar copper alloy is adopted in the water cooled part of anodes for electric arc furnaces, where the scrap steel is melted[11]. Cyclic hardening material models are also of interest for the simulation of cyclic thermal shocks in steel parts[12], and can be used, for instance, to develop numerical analyses for life prediction in tool steel[13]. Automotive component design can also benefit from accurate simulations with thermo-mechanical loads, as suggested in[14].

Section 2 describes the experimental tests. Section 3 outlines the equations for time-independent material plasticity, in order to summarise the main parameters involved in the experimental identification discussed in Section 4.

2. Experimental testing

In the experimental tests, CuAg alloy specimens (as per ASTM B 124)[15] were subjected to isothermal strain-controlled cyclic tests at three different temperatures (room temperature, 250

°C, 300 °C).[16] The tests applied a saw-tooth fully-reversed (R_ε=-1) strain waveform at a strain rate of 0.01 s^{-1}, which also enabled the creep effect to be reduced considerably.[17]

Specimens had a cylindrical un-notched geometry, with a smooth variation with a diameter from 12 mm to 7 mm, and a large fillet radius (40 mm) to prevent a stress concentration in the transition region. Specimens had a total length of 120 mm and a gauge length of 20 mm, see Figure 1(a).

Tests at room temperature (RT) were carried out on a servo-hydraulic Instron-Schenck test rig, with a nominal force of ±250 kN. Specimens were clamped by mechanical grips; an Instron extensometer (with a 12.5 mm gauge length and range ±5 mm) was used to record the longitudinal elongation during testing, see Figure 1(b). A total of 10 specimens were tested at room temperature (20 °C). An anomalous testing behaviour occurred in two specimens (e.g. crack initiated by the extensometer, specimen bending) and caused distorted results, which were discarded from subsequent analyses.

High temperature tests were carried out by an Instron test rig with a nominal force of ±100 kN. Specimens were heated by an induction heating system (coil) with a 10 kW medium frequency generator, Hüttinger TIG 10/300. The specimen temperature, measured within the gauge length with a pre-stressed type K loop thermocouple, was kept constant all the time and nearly uniform within the gauge length. An extensometer (with a 12.5 mm gauge length and range ±1.8 mm) was used to record the longitudinal elongation. Test specimens were clamped to water-cooled hydraulic grips, see Figure 1(c). Thermal strain compensation was also performed before starting the test to prevent unwanted thermal stress.

A total of 10 and 8 specimens were tested at 250 °C and 300 °C, respectively. Similarly to RT tests, also at high temperatures some specimens showed an anomalous behaviour during testing (e.g. specimen destroyed when the test started, problems with clamping) and their results were excluded from subsequent analyses. For each temperature, a total of seven specimens remained for the subsequent analyses.

At each testing temperature, specimens were subjected to strain amplitudes ε_a from 0.15% to 0.7%. The applied strain ε and resulting axial stress σ were recorded throughout each test (approximately 200 points per cycle), thus enabling the shape of the stress-strain cycles to be described in detail. Tests were interrupted before the complete failure of the specimen, when the maximum stress σ_{max} had decreased by 80% from its initial value. At the end of the test, the number of cycles to failure N_f was also registered. Figure 2 plots examples of experimental (first and stabilised) cycles at room temperature.

3. Plasticity models: theoretical background

The modelling of rate-independent elasto-plastic material behaviour under cyclic loading can be well represented by a combined kinematic and isotropic hardening model (see Figure 3), in which the von Mises yield surface is expressed as:[3,4,5]

$$\sqrt{\frac{3}{2}(\boldsymbol{S}-\boldsymbol{X}):(\boldsymbol{S}-\boldsymbol{X})}-R-\sigma_{y0}=0 \qquad (1)$$

where $\boldsymbol{S}$ is the deviatoric stress tensor, $\boldsymbol{X}$ is the back stress (kinematic) tensor, R is the drag stress, and σ_{y0} is the initial yield stress. The back stress $\boldsymbol{X}$ controls the translation of the yield surface (kinematic model), whereas the drag stress R controls the homothetic expansion (isotropic model) of the yield surface during cyclic loading.

Different models have been proposed to relate back stress $\boldsymbol{X}$ to plastic strain.[3,4,5] In Prager's linear kinematic model, $\boldsymbol{X}$ is proportional to the plastic strain increment:

$$\mathrm{d}\boldsymbol{X}=\frac{2}{3}C\mathrm{d}\boldsymbol{\varepsilon}_{pl} \qquad (2)$$

where C is the hardening modulus. The linear kinematic model was modified by Armstrong and Frederick (AF) by adding a recall term:[18]

$$\mathrm{d}\boldsymbol{X}=\frac{2}{3}C\mathrm{d}\boldsymbol{\varepsilon}_{pl}-\gamma\,\boldsymbol{X}\,\mathrm{d}\varepsilon_{pl,acc} \qquad (3)$$

which depends on the accumulated plastic strain $\varepsilon_{pl,acc}=\left(2/3\,d\boldsymbol{\varepsilon}_{pl}:d\boldsymbol{\varepsilon}_{pl}\right)^{1/2}$. In expression (3), the recall constant γ controls the decrease rate of the hardening modulus as the plastic strain accumulates. A better approximation is achieved by decomposing the back-stress into several AF models (Chaboche model):[3,4,5]

$$\boldsymbol{X}=\sum_i \boldsymbol{X}_i \quad , \quad \mathrm{d}\boldsymbol{X}_i=\frac{2}{3}C_i\,\mathrm{d}\boldsymbol{\varepsilon}_{pl}-\gamma_i\,\boldsymbol{X}_i\,\mathrm{d}\varepsilon_{pl,acc} \qquad (4)$$

Generally, up to three pairs of kinematic parameters (C_i, γ_i) are sufficient to represent the behaviour of the material over a wide range of strains (each one covering a specific range of strains). The coefficients of the material (C_1, γ_1) can be used to describe the initial non-

linearity at small strain, (C_2, γ_2) the non-linear behaviour at medium to large strain, whereas (C_3, γ_3) describes the asymptotic behaviour at large strain (ε>1%).

Under uniaxial loading, the AF kinematic model provides a simple analytical solution after the direct integration of Eq. (3):[3,4,5]

$$X = \nu\frac{C}{\gamma} + \left(X_0 - \nu\frac{C}{\gamma}\right)e^{-\nu\gamma\left(\varepsilon_{\mathrm{pl}} - \varepsilon_{\mathrm{pl},0}\right)} \tag{5}$$

where X_0, $\varepsilon_{\mathrm{pl},0}$ are the values of X and $\varepsilon_{\mathrm{pl}}$ at the last change in plastic strain rate, whereas ν=±1 depending on the direction of the plastic flow. Similarly, for the Chaboche model:

$$X = \sum_{\mathrm{i}}\left[\nu\frac{C_{\mathrm{i}}}{\gamma_{\mathrm{i}}} + \left(X_0 - \nu\frac{C_{\mathrm{i}}}{\gamma_{\mathrm{i}}}\right)e^{-\nu\gamma_{\mathrm{i}}\left(\varepsilon_{\mathrm{pl}} - \varepsilon_{\mathrm{pl},0}\right)}\right] \tag{6}$$

In stabilised cycles, the amplitudes of stress σ_{a} and plastic strain $\varepsilon_{\mathrm{pl,a}}$ are related as:

$$\sigma_{\mathrm{a}} = \sigma_{\mathrm{yc}} + \sum_{i=1}\frac{C_i}{\gamma_i}\tanh\left(\gamma_i\varepsilon_{\mathrm{pl,a}}\right) \tag{7}$$

In the isotropic model, the change in drag stress R depends on the accumulated plastic strain by the differential equation (often called Voce's model[19]):

$$\mathrm{d}R = b\left(R_\infty - R\right)\mathrm{d}\varepsilon_{\mathrm{pl,acc}} \tag{8}$$

where b is the speed of stabilization, R_∞ is the asymptotic drag stress at cyclic stabilisation (R_∞ is positive or negative to represent either hardening or softening). Direct integration of (8) gives the exponential relationship:

$$R = R_\infty\left(1 - e^{-b\varepsilon_{\mathrm{pl,acc}}}\right) \tag{9}$$

The change of R from zero to R_∞ measures the amount of hardening or softening in cyclic loading. This trend can also be quantified by the change in maximum stress $\sigma_{\mathrm{max,i}}$ after N cycles, relative to the maximum stress in the first cycle $\sigma_{\mathrm{max,1}}$ and in the stabilised one $\sigma_{\mathrm{max,s}}$:

$$\frac{\sigma_{\max,i}-\sigma_{\max,1}}{\sigma_{\max,s}-\sigma_{\max,1}} \cong \frac{R}{R_\infty} = 1-e^{-b\varepsilon_{pl,acc}} \tag{10}$$

The ratio on the left-hand side of Eq. (10) always remains positive, also for materials that exhibit softening ($\sigma_{\max,s} \leq \sigma_{\max,1}$ and $\sigma_{\max,i} \leq \sigma_{\max,1}$). In strain-controlled cycling, the accumulated plastic strain after N cycles is approximated as $\varepsilon_{pl,acc} \cong 2\Delta\varepsilon_{pl,a} N$, where $\Delta\varepsilon_{pl}=2\varepsilon_{pl,a}$ is the plastic strain range (twice the amplitude) which is taken as nearly constant in each cycle.

Expression (10) assumes that hardening or softening only depends on the amount of accumulated plastic strain, irrespectively of the actual value of plastic strain amplitude $\varepsilon_{pl,a}$ (this assumption will be contradicted by the data for the CuAg alloy shown later). In strain-controlled cycles, stabilisation then occurs earlier (lower N) in cycles with a larger plastic strain amplitude $\varepsilon_{pl,a}$. If two cycles have different amplitudes $(\varepsilon_{pl,a})_1 > (\varepsilon_{pl,a})_2$, stabilisation occurs at different numbers of cycles $N_1 < N_2$, while the accumulated plastic strain reached in both cases remains identical ($4(\varepsilon_{pl,a})_1 \cdot N_1 = 4(\varepsilon_{pl,a})_2 \cdot N_2$).

When combined, the kinematic and isotropic models provide the stress:

$$\sigma(\varepsilon_{pl,acc}) = \sigma_{y0} + X(\varepsilon_{pl,acc}) + R(\varepsilon_{pl,acc}) \tag{11}$$

at a certain amount of accumulated plastic strain $\varepsilon_{pl,acc}$ reached after N cycles, where $X(\varepsilon_{pl,acc})$ and $R(\varepsilon_{pl,acc})$ are the corresponding values of back stress and drag stress.

4. Identifying material parameters from experiments

This section explains how the material parameters were identified by fitting experimental data. The unknown material parameters are: the elastic modulus E, the initial yield stress σ_{y0}, the kinematic variables C_i, γ_i (with i=1,2, or 3, depending on the back-stress decomposition) and the isotropic variables R_∞, b.

As suggested in Ref. [3], parameters of kinematic and isotropic models can be identified separately and sequentially: kinematic variables from stabilised cycles, and isotropic variables from the time evolution of stress-strain cycles. In fact, the kinematic model stabilises after a few cycles,[3,4,5] during which the isotropic model contributes little to strain hardening/softening, due to the relatively small amount of accumulated plastic strain. On the other hand, in subsequent cycles the strain hardening/softening is essentially controlled by the isotropic model.

4.1. Elastic modulus

The elastic modulus E must be estimated first, as it defines the material elastic response, which is required for the subsequent identification of the yield stress and plastic strain. Correctly estimating the elastic modulus is thus very important for accurately defining the elasto-plastic material response.[20]

As suggested in Refs. [20,21], the elastic modulus was estimated by a least squares linear fitting on the cyclic stress-strain data recorded at different strain amplitudes and temperatures. Since the elastic modulus may vary during the cyclic test,[20] two different moduli (symbols E_1, E_s) were estimated. The value E_1 was determined from the straight line portion of the first one-quarter cycle, at the start of the cyclic test. The value E_s was estimated from the stabilised cycle, which usually occurs approximately at half the number of cycles to failure. The value E_s was taken as the modulus E_{up} in the loading portion of the stabilised cycle, since the difference between E_{up} and E_{down} (value in the unloading portion of the stabilised cycle) was less than 10%. Values of E_1 and E_s measured for each strain amplitude were used in the subsequent analysis step to determine the yield stress.

Table 1 lists the values of E_1 and E_s estimated from the test data at each temperature and strain amplitude (data with an anomalous testing behaviour were excluded, as previously highlighted). Within this set, a few values (marked by 'a') were not considered in the statistical analysis, because they were actually estimated from the second cycle due to some disturbance occurring at the beginning of the test.

For each temperature, the last rows in Table 1 report the mean values, the standard deviations and 95% confidence intervals for the mean value, for both parameters of E_1 and E_s.

Though unnecessary for the subsequent analysis, a statistical analysis was also performed to investigate whether the elastic modulus follows a trend with temperature. The theoretical details are not reported here, as they can be found in any introductory statistical textbook (for example Ref. [26]). The results are summarised in the Appendix and Table 5. The statistical analysis emphasises that both E_1 and E_s markedly decrease from room temperature to 250 °C, whereas they remain almost stable from 250 °C to 300 °C (which may be expected, as these temperatures are much closer).

In the following, the symbols $E_{1,ave}$, $E_{s,ave}$ are used to indicate the mean values that will be used in the numerical simulations.

4.2. Yield stress

Once the elastic modulus was determined, the yield stress was estimated. There are two distinct values: initial yield stress σ_{y0} measured at the first one-quarter cycle, and cyclic yield stress σ_{yc} measured at the stabilised cycle. The initial and cyclic yield stresses were determined for each strain amplitude by considering the corresponding values of E_1 and E_s, respectively.

From the stress σ and total strain ε recorded in each test, the components of elastic strain $\varepsilon_{el}=\sigma/E$ and plastic strain $\varepsilon_{pl}=\varepsilon-\varepsilon_{el}$ were separated. In each measured cycle, the total strain amplitude ε_a was also separated into the elastic $\varepsilon_{el,a}$ and plastic $\varepsilon_{pl,a}$ strain components.

The initial yield stress σ_{y0} corresponds to the onset of plastic strain, i.e. it is the point where the stress first deviates from the vertical axis of the stress vs. plastic strain plot, see Figure 4(a). The cyclic yield stress σ_{yc} was determined by imposing a 0.02% strain offset from the tip of the loading portion of the stress vs. plastic strain stabilised cycle. The intersection gives $2\sigma_{yc}$ (i.e. twice the cyclic yield stress), see Figure 4(b).

Table 2 gathers the yield stresses estimated at each temperature. For each temperature, the last rows in Table 2 report the mean values, the standard deviations and 95% confidence intervals for the mean value, for both parameters σ_{y0} and σ_{yc}.

The change in yield stress from the first to the stabilised cycle reveals whether the material is hardening or softening. Table 2 reveals that $\sigma_{yc}<\sigma_{y0}$ in all cases examined, which confirms that the CuAg alloy softens.

As for the elastic modulus, a statistical analysis was used to detect if the yield stress also follows a temperature trend (see Appendix and Table 5). While σ_{y0} does not seem to be influenced by the temperature, the cyclic yield stress σ_{yc} decreases from room temperature to 250 °C. Instead, no marked trend is detected for both σ_{y0} and σ_{yc}, when the temperature increases from 250 °C to 300 °C.

In the following, the symbols $\sigma_{y0,ave}$ and $\sigma_{yc,ave}$ are used to indicate the mean values that will be used in the numerical simulations.

4.3. Kinematic model

Kinematic parameters were identified from stabilised cycles at various plastic strain amplitudes. The parameters obtained thus well represent the material behaviour over a wide range of strain amplitudes.

The procedure is explained here for the room temperature data. First, the amplitudes of stress σ_a and plastic strain $\varepsilon_{pl,a}$ were measured for each stabilised cycle available. The amplitude of back stress is $X_a=\Delta X/2=\sigma_a-\sigma_{yc}$ where σ_{yc} has already been determined. Figure 5 depicts an example for three cycles.

The above calculation steps were repeated for each stabilised cycle and resulted in a set of pairs $(\varepsilon^{(j)}_{pl,a}, X_a^{(j)})$ plotted in Figure 6. These data correspond to the tip of each stabilised cycle. The experimental points were then fitted by the kinematic model in (7) with one-pair (C_1, γ_1), two-pairs (C_1, γ_1, C_2, γ_2), or three-pairs (C_1, γ_1, C_2, γ_2, C_3, γ_3).

The fitting procedure described above was also applied to the stabilised cycles at 250 °C and 300 °C, and resulted in the parameters listed in Table 3.

Compared to the one-pair model, the two- and three-parameter models best describe the experimental point trend in Figure 6 (the three-parameter model actually gives the smallest fitting error).

The validity of the parameters identified was also verified by checking simulations against experiments for several stabilised cycles at different temperatures and strain amplitudes. Simulations only used a kinematic model with one, two or three pairs (C_i, γ_i), whose values are taken from Table 3. For the elastic modulus and the cyclic yield stress, simulations took the average values $E_{s,ave}$, $\sigma_{yc,ave}$ previously calculated.

The results in Figure 7 and Figure 8 emphasise that a close agreement with the experiments in Figure 6 does not necessarily also imply a close agreement between simulated and experimental cycles.

Figure 7 compares three stabilised cycles with the same strain range ε_a=0.5%, but with different temperatures. Overall, the results of the three-pair seem slightly closer to the experiments, although with some deviations. Surprisingly, at all three temperatures, the one-pair model follows the unloading branch of cycles better than the other two models. The two-pair model, instead, seems to provide the worst prediction, especially at 250 °C and 300 °C where it moves away from the curved branch of experimental cycles. Likewise for all three models, the fitting tends to become less satisfactory in the curved branch of each cycle, close to the "knee" point dividing the elastic and plastic domains. At the knee point, for example, the experimental cycles have a smoother shape than the simulations. In addition, in the curved branch, the shape of the simulated cycles is governed by exponential equation (6), thus possibly resulting in a poor prediction despite the accuracy of fitting achieved in Figure 6, which in fact only refers to the tip of the saturated cycles.

Similar considerations also apply to Figure 8, which compares the stabilised cycles at the same temperature (RT), but different strain amplitudes ε_a=0.3%, 0.4%, 0.6%. The average values $E_{s,ave}$=114763 MPa, $\sigma_{yc,ave}$=86 MPa from Table 1 and Table 2 were used. The observed agreement confirms how, regardless of the number of pairs, the kinematic model correctly simulates the shape of the stabilised cycles also over a wide interval of strain ranges, at room temperature. Similar conclusions also apply to cycles at higher temperatures.

In conclusion, based on the above comparison, the three-pair model was used as a reference in all subsequent simulations using the combined kinematic-isotropic model exclusively because it gives the lowest fitting error (see Figure 6). However, simulations with models with one, two or three pairs show small differences that would probably be hidden, if the scatter among tests at a constant strain range were also taken into account. It can therefore be concluded that, in most cases the one-parameter model might be preferable due to its lower number of parameters. As a consequence, the model complexity will be reduced and, even if only slightly, also the computational time.

The kinematic model should be adopted to describe the shape of the stress-strain loop and the Bauschinger effect, however it does not capture the evolution of cyclic hardening/softening. Figure 9 shows a comparison between the experimental (first and stabilised) and the first five cycles obtained by the numerical simulation, which exploits a three-pair kinematic model with either initial ($E_{1,ave}$, $\sigma_{y0,ave}$) or stabilised ($E_{s,ave}$, $\sigma_{yc,ave}$) values for Young's modulus and yield stress.

The kinematic model with initial parameters stabilises over the first two cycles, showing a quite good agreement with the first experimental cycle. Nevertheless, it does not further evolve toward the stabilised experimental cycle. Similarly, if the stabilised parameters are adopted from the beginning of the simulation, the kinematic model overlaps with the stabilised experimental loop (as can be deduced from Figure 7). In the case in which strain softening occurs, yielding occurs at a lower stress value, thus leading to a greater amount of plastic strain. As a result, as also pointed out in [22], when simulating the cyclic response of an actual mechanical component, using stabilised parameters in the kinematic model would produce plastic deformations in regions which actually should remain elastic without exhibiting any softening phenomenon, thus leading to possible mistakes in the final results. In order to take the cyclic hardening/softening into account, an isotropic model should then be combined with a kinematic one.

4.4. Isotropic model

The next step is to identify the isotropic parameters. Figure 10 plots the change in the maximum stress σ_{max} in each cycle, as a function of the cycle number N, for room temperature data at several strain amplitudes. The decreasing trend confirms a softening behaviour for the CuAg alloy, which also occurs for data at 250 °C and 300 °C.

However the CuAg alloy never saturates completely: the maximum stress σ_{max} continues to decrease and does not approach any horizontal asymptote at large N. Consequently, the minimum value of σ_{max} in the last cycle, which defines the saturated stress $\sigma_{max,s}$, needs to be interpreted in a conventional way (saturated stress is then identified at half cycles to failure). The total excursion of σ_{max} from its first value $\sigma_{max,1}$ in the first cycle to the saturated stress $\sigma_{max,s}$ defines the asymptotic drag stress $R_\infty=\sigma_{max,1}-\sigma_{max,s}$ in Eq. (9).

The second distinctive feature is that, at certain strain amplitudes (for example, ε_a=0.175% at room temperature), the CuAg alloy slightly hardens in the first few cycles, before it starts to soften significantly. As a result, the trend of maximum stress is not monotonic. Instead, it first increases in the first few cycles so that $\sigma_{max,i}>\sigma_{max,1}$ and negative values result in the left hand side in Eq. (10).

Finally, the data in Figure 10 (as well as those at 250 °C and 300 °C, although not shown here) highlight that although the maximum stress σ_{max} increases predictably with strain amplitude values, the curves are not simply shifted based on strain amplitudes. Not only are such curves characterised by different "shapes" (some are more flat, others more arched), some of them also intersect each other. This demonstrates that the curves are not simply shifted upward or downward as the strain amplitude increases or decreases. As a result, the difference $R_\infty=\sigma_{max,1}-\sigma_{max,s}$ takes dissimilar values for each strain amplitude, as shown in Table 4, which also in the last row reports the R_∞ averaged over all strain amplitudes, for each testing temperature.

These three distinctive features have important consequences when trying to estimate the exponent b of the isotropic model by fitting Eq. (10) to the experiments. This fitting requires that the σ_{max}/N curves in Figure 10 are rearranged by drawing the left-hand side in (10) as a function of the plastic strain accumulated after N cycles $\varepsilon_{pl,acc} \cong 2\Delta\varepsilon_{pl,a}N$, where $2\Delta\varepsilon_{pl,a}$ approximates the amount accumulated in one cycle. This calculation results in the "s-shaped" data in Figure 11.

Essentially, Figure 10 and Figure 11 both show the same data, mirrored about a horizontal axis and scaled in both the y-axis (dimensionless maximum stress) and x-axis (from N to $\varepsilon_{pl,acc}$). The data in Figure 11 thus have the same distinctive features already observed in Figure 10.

First, for some plastic strain amplitudes, data take on negative values for an accumulated plastic strain in the range $10^{-2} \div 5 \cdot 10^{-2}$. These negative values are caused by the small hardening that occurs over the first 5-10 cycles (just after starting the test), before the material starts to soften significantly. Such a small hardening gives a higher maximum stress $\sigma_{max,i}$ than the initial one $\sigma_{max,1}$ in the very first cycle, which results in a positive difference $\sigma_{max,i} - \sigma_{max,1}$ and thus a negative ratio in the left-hand side of Eq. (10).

Second, the data in Figure 11 do not converge to any horizontal asymptote at large values of accumulated plastic strain. They even seem not to converge at all. When approaching large values of accumulated plastic strain (around $\varepsilon_{pl,acc}=4 \div 8$), data still increase with a positive slope (see, for example, the series at $\varepsilon_a=0.175\%$, 1%, 1.25%). Also in the region at low $\varepsilon_{pl,acc}$ (close to 10^{-2}), the data points do not stay horizontal, but increase almost immediately with a positive slope (for example, in Figure 11 see series for $\varepsilon_a=0.2\%$ and 0.4%).

However a third aspect is more significant: the curves in Figure 11 depend on the values of plastic strain amplitude $\varepsilon_{pl,a}$, which contradicts the hypothesis behind Eq. (10) in which material softening is assumed to only depend on the accumulated plastic strain, regardless of the actual value of plastic strain amplitude. This hypothesis implies that all experimental data should collapse into one single curve. In Refs. [3,4,5], this hypothesis is verified against the cyclic data of a 316 stainless steel in Ref. [23] (these data can also be found in Refs. [3,4,5]), although careful examination would reveal that a slight dependence on strain amplitude also characterises this material. A much stronger dependence has been observed, instead, for other materials (nickel base superalloy[24], 42CrMo4 steel[25]) investigated in two independent studies.

The features mentioned above help to explain why trying to fit expression (10) to the data in Figure 11 cannot be fully successful. For example, Eq. (10) presumes that the data do not depend on the strain amplitude values, whereas they actually do. This dependence is confirmed by the dissimilar values of b in Table 4, which result from fitting Eq. (10) separately to data pertaining to different strain amplitudes. These differences then suggest that model (8) should be modified to account for plastic strain amplitude explicitly (this, of course, falls outside the scope of this article).

Fitting also does not seem completely satisfactory when restricted to data at only one strain amplitude, as in the examples in Figure 12 for single data series at ε_a=0.3% and 0.5%. In fact, Eq. (10) is always positive and has two horizontal asymptotes at both tails, which is not shown in the data. A similar trend is also observed for high temperature data.

The experimental outcome shows that the CuAg alloy exhibits a variability of such parameters over a wide range of strains. Attempting to fit the isotropic model separately to data at each strain amplitude would result in the parameters listed in Table 4.

On the other hand, only one single value of the isotropic parameters is needed in order to use the isotropic model in a numerical simulation. In addition, thermo-mechanically loaded components usually undergo plastic deformations over a wide range of strains. Therefore, not only does the material model to be adopted in simulations need to be calibrated for each strain amplitude, but it should also be valid over a wider range of loading conditions. A possible compromise could be to take an average value $R_{\infty,ave}$ and to estimate a single value b_{all} by fitting Eq. (10) to all the experimental data as in Figure 11.

Note that the value of b governs the speed of stabilisation, but not the final shape of the stabilized cycle. In fact, the typical strategy suggested in the literature[22] to speed up the simulation is to increase the value of this parameter.

4.5. Combined kinematic and isotropic model

The final step is to combine the isotropic with the kinematic model in order to verify whether numerical simulations can reasonably capture the material softening over cycles.

For instance, in Figure 13 the combined kinematic-isotropic model is compared to 80 experimental cycles at room temperature and strain amplitude ε_a=0.5% (for more clarity, only one cycle every five is shown). Simulations used the material parameters presented in Table 3 and Table 4. Although the parameters are not specifically calibrated on the considered strain amplitude, the first and stabilised cycles, as well as the overall cycle evolution, are well represented. By contrast, if only one strain amplitude is of interest, the values in Table 4 permit the isotropic component of the combined model to be calibrated on the desired condition.

5. Conclusions

The elasto-plastic cyclic response of a CuAg0.1 alloy for thermo-mechanical applications was investigated. Strain-controlled cyclic tests were performed at three different temperatures

(room temperature, 250 °C, 300 °C) and at several strain amplitudes. The stress-strain responses recorded during tests were used to identify several material parameters: elastic modulus and yield stress (initial and stabilised), parameters of non-linear kinematic and isotropic models (Armstrong-Frederick, Chaboche, Voce).

Each first cycle provided the initial yield stress σ_{y0} and the elastic modulus E_1, whereas stabilised cycles provided the cyclic yield stress σ_{yc} and the elastic modulus E_s at saturation. Stabilised cycles at several strain amplitudes provided the basis for identifying parameters of the kinematic model with one, two or three pairs (C_i,γ_i). The evolution of stress-strain cycles until complete stabilisation was used for estimating the isotropic parameters R_∞, b. All parameters were evaluated from data at each testing temperature. Finally, the validity of all the identified material parameters was checked by comparing simulated against experimental cycles.

The kinematic model correctly captured the behaviour of the material in stabilised conditions. Although kinematic models with one, two or three pairs showed slight differences, the three-pair model was chosen as reference in all simulations, since it gave the lowest fitting error. However, as the scatter among tests may be relevant, it can be concluded that the one-pair model may be preferable due to its lower number of parameters.

The kinematic model is suitable for describing the shape of the stress-strain loop, but it does not capture the evolution of cyclic softening of the CuAg0.1 alloy. Thus, an isotropic model was combined with the kinematic one. The attempt to fit this model to the experimental data was, however, not as satisfactory as expected, due to some peculiarities of the data. Indeed, the decrease in the maximum stress σ_{max} over cycles was shown to be correlated not only to the accumulated plastic strain $\varepsilon_{pl,acc}$, but also to the strain amplitude ε_a, thus leading to an uncertainty when estimating the speed of stabilisation b. Despite such peculiarities seeming to contradict some of the assumptions behind the isotropic model, the combined model (kinematic plus isotropic) permits the first and stabilised cycles to be represented quite well. The combined model also captures the material softening over cycles with reasonable accuracy despite the determination of b parameter being affected by the previously mentioned uncertainty.

The results collected in this work summarise all the necessary data required by a commercial finite element code, used to perform cyclic elasto-plastic simulations aimed at structural durability analysis.

6. Appendix – Statistical analysis of data

A statistical test based on the analysis of variance (ANOVA) can be performed on the experimental data to detect whether the elastic modulus and the yield stress are in some way dependent on the temperature. The data in Table 1 and Table 2 are treated as a single-factor experiment, in which the factor (temperature) varies at three levels (RT, 250 °C, 300 °C).

In a single-factor ANOVA, hypothesis testing is performed on a "null hypothesis" H_0, which assumes that data at different temperatures share the same mean value (i.e. the temperature has no effect on data). If the test rejects H_0, there is strong evidence that the parameter (elastic modulus or yields stress) is actually affected by the temperature.

The result of the test is summarised by a *p*-value, which needs to be compared with the significance level of the test α (the typical value α=0.01 is selected here). The *p*-value conveys the information on the weight of evidence against H_0: if the data return a *p*-value that is considerably smaller than α, then there is strong evidence to conclude that H_0 is not true (i.e. the data are affected by the temperature). Table 5 reports the *p*-values resulting from the hypothesis testing of the data in Table 1 and Table 2. The analysis compares the data either for all three temperatures, or just for 250 °C and 300 °C.

A dependence on temperature was detected in all the cases examined, except for σ_{y0}. This dependence is, however, limited to a change in temperature from room condition to 250 °C, whereas no appreciable variation occurred from 250 °C to 300 °C (a *p*-value>α was always observed when only data at 250 °C and 300 °C were analysed).

References

1 Li, G., Thomas, B.G. and Stubbins, J.F. (2000) Modeling creep and fatigue of copper alloys. *Metall Mater. Trans. A*, **31A**, 2491–2502.

2 Srnec Novak, J., Stanojevic, A., Benasciutti,D., De Bona F. and Huter, P. (2015) Thermo-mechanical finite element simulation and fatigue life assessment of a copper mould for continuous casting of steel. *Procedia Engineering*, **133**, 688–697.

3 Lemaitre, J. and Chaboche, J.L. (1990) *Mechanics of solid materials*. Cambridge University Press, Cambridge, UK.

4 Chaboche, J.L. (1986) Time-independent constitutive theories for cyclic plasticity. *Int. J. Plasticity*, **2(2)**, 149–188.

5 Chaboche, J.L. (2008) A review of some plasticity and viscoplasticity constitutive theories. *Int. J. Plasticity*, **24**, 1642–1693.

6 Khan, A.S. and Huang, S. (1995) *Continuum theory of plasticity*. John Wiley & Sons, New York, USA.

7 Chen, W.F. and Zhang, H. (1988) Plasticity for structural engineers, Springer-Verlag, New York, NY, USA.

8 Benasciutti, D. (2012) On thermal stress and fatigue life evaluation in work rolls of hot rolling mill. *J. Strain Anal. Eng. Des.*, **47(5)**, 297-312.

9 Benasciutti, D., De Bona, F. and Munteanu, M.Gh. (2015) An harmonic 1D-element for non linear analysis of axisymmetric structures: The case of hot rolling. Proc. of 1st Pan-American Congress on Computational Mechanics (PANACM 2015) and 11th Argentine Congress on Computational Mechanics (MECOM 2015), Buenos Aires, 27-29 April 2015, pag. 1566-1577.

10 Benasciutti, D., De Bona, F. and Munteanu, M.Gh. (2016) A harmonic one-dimensional element for non-linear thermo-mechanical analysis of axisymmetric structures under asymmetric loads: The case of hot strip rolling. *J. Strain Anal. Eng. Des.*, **51(7)**, 518-531.

11 Moro, L., Benasciutti, D., De Bona, F. and Munteanu, M.Gh. (2017) Simplified numerical approach for the thermo-mechanical analysis of steelmaking components under cyclic loading: an anode for electric arc furnace. *Ironmak. Steelmak.*, published on line (doi: 10.1080/03019233.2017.1339482).

12 Janssens, K.G.F (2011) Case study of the applicability of cyclic hardening material descriptions in finite element simulation of cyclic thermal shocks. *Fatigue Fract. Engng. Mater. Struct.*, 34, 562-572.

13 Berti, G.A., Monti, M. (2009) Improvement of life prediction in AISI H11 tool steel by integration of thermo-mechanical fatigue and creep damage models. *Fatigue Fract. Engng. Mater. Struct.* **32**, 270-283.

14 Thomas, J.J., Verger, L., Bignonnet, A. and Charkaluk, E. (2004) Thermomechanical design in the automotive industry, *Fatigue Fract. Engng. Mater. Struct.* **27**, 887-895.

15 ASTM B 124 - B 124M (2008) Standard specification for copper and copper alloy forging rod, bar, and shapes.

16 Srnec Novak, J., Benasciutti, D., De Bona, F., Stanojevic, A., De Luca, A. and Raffaglio, Y. (2016) Estimation of material parameters in nonlinear hardening plasticity models and strain life curves for cuag alloy. *IOP Conf. Series: Materials Science and Engineering*, **119**, 012020.

17 Rouse, J.P., Hyde, C.J., Sun, W. and Hyde, T.H. (2013) Comparison of several optimisation strategies for the determination of material constants in the Chaboche visco-plasticity model. *J. Strain Anal. Eng. Des.*, **48(6)**, 347-63.

18 Armstrong P.J., Frederick C.O. A mathematical representation of the multiaxial Bauschinger effect. Report RD/B/N731, Central Electricity Generating Board (CEGB), 1966 (reprinted in: Frederick C.O., Armstrong P.J. (2007) A mathematical representation of the multiaxial Bauschinger effect. *Mater High Temp.* **24**(1), 1–26).

19 Voce, E. (1955) A practical strain hardening function. *Metallurgia*, **51**, 219-26.

20 Hales, R., Holdsworth, S.R., O'Donnell, M.P., Perrin, I.J. and Skelton, R.P. (2002) A Code of Practice for the determination of cyclic stress-strain data. *Mater. High Temp.*, **19(4)**, 165-185.

21 International Standard – ISO 12106 (2003). Metallic materials – Fatigue testing – Axial – strain – controlled method.

22 Chaboche, J.L. and Cailletaud, G. (1986) On the calculation of structures in cyclic plasticity or viscoplasticity. *Comput. Struct.*, **23**(1), 23-31.

23 Goodall, I.W., Hales, R. and Walters, D.J. (1980) On constitutive relations and failure criteria of an austenitic steel under cyclic loading at elevated temperature. In: IUTAM Symp. Creep in Structures, Leicester, UK. Springer-Verlag (eds.: Ponter, A.R.S. and Hayhurst, D.R.), pag. 103-127.

24 Zhao, L.G., Tong, B., Vermeulen, B. and Byrne, J. (2001) On the uniaxial mechanical behaviour of an advanced nickel base superalloy at high temperature. *Mech. Mater.*, **33**, 593-600.

25 Basan, R., Franulović, M., Prebil, I. and Kunc, R. (2017) Study on Ramberg-Osgood and Chaboche models for 42CrMo4 steel and some approximations. *J. Constr. Steel Res.*, **136**, 65-74.

26 Montgomery, D.C. and Runger, G.C. (2014) *Applied statistics and probability for engineers*, 6th ed. John Wiley & Sons, Hoboken, NJ, USA.

TABLES

Table 1. Elastic modulus estimated from cyclic stress-strain data at different temperatures. For each strain amplitude ε_a, the elastic modulus is estimated from the first cycle, E_1, and from the stabilised cycle, E_s. The last rows list the mean value, standard deviation and 95% confidence interval on the mean.

	Room temperature		250 °C		300 °C	
ε_a	E_1 (MPa)	E_s (MPa)	E_1 (MPa)	E_s (MPa)	E_1 (MPa)	E_s (MPa)
0.15%.	122400	116400	106200[a]	97110	–	–
0.175%	122000	114500	–	–	107700[a]	94000
0.2%	121500	115900	108200[a]	99910	100400[a]	96990
0.25%	–	–	–	–	102600[a]	92350
0.3%	119700	116900	108500	93760	105600	97930
0.35%	–	–	108600	98530	–	–
0.4%	119900	115900	113400[a]	98760	104300	98820
0.5%	118200	113500	105400	90140	101900	95770
0.6%	117400	110100	–	–	–	–
0.7%	118800	114900	103900	85100	103400	87690
Mean value	119988	114763	106600	94759	103800	94793
Standard deviation	1834	2180	2334	5445	1556	3849
Confidence interval	118454÷121521	112940÷116585	102886÷110314	89722÷99795	101325÷106275	91233÷98353

[a] Values estimated on the second cycle and then not included in the statistical analysis

Table 2. Yield stress estimated from several stress-strain cycles at different temperatures. For each strain amplitude ε_a, the table gives the initial yield stress σ_{y0} (estimated from the first cycle) and the cyclic yield stress σ_{yc} (estimated from the stabilised cycle). The last rows list the mean value, standard deviation, and 95% confidence interval on the mean.

	Room temperature		250 °C		300 °C	
ε_a	σ_{y0} (MPa)	σ_{yc} (MPa)	σ_{y0} (MPa)	σ_{yc} (MPa)	σ_{y0} (MPa)	σ_{yc} (MPa)
0.15%.	51	73	116[a]	52	–	–
0.175%	90	74	–	–	113	48
0.2%	96	72	135	55	132[a]	49
0.25%	–	–	–	–	83[a]	53
0.3%	122	88	126	60	124	53
0.35%	–	–	116	60	–	–
0.4%	139	91	104[a]	61	103	55
0.5%	118	84	85	57	116	49
0.6%	135	89	–	–	–	–
0.7%	155	114	87	53	82	44
Mean value	113	86	110	57	108	50
Standard deviation	33.1	13.8	22.8	3.6	16.2	3.8
Confidence interval	85.5÷141.0	74.1÷97.2	81.5÷138.1	53.5÷60.2	87.5÷127.7	46.7÷53.6

[a] Values estimated on the second cycle and then not included in the statistical analysis

Table 3. Kinematic parameters identified from experimental data (values of C_i are in MPa).

Temperature	One pair		Two pairs				Three pairs					
	C_1	γ_1	C_1	γ_1	C_2	γ_2	C_1	γ_1	C_2	γ_2	C_3	γ_3
RT	51140	702.4	62500	2051	15060	292.2	25880	1627	24460	1624	15620	315.4
250 °C	40060	915.8	87650	3437	6070	48.5	31310	1708	10240	343.6	5256	1748
300 °C	32660	737.3	81650	3191	5502	0	13170	1092	10700	398.2	10650	1155

Table 4. Isotropic parameters identified from experiments.

	Room temperature		250 °C		300 °C	
ε_a	b	R_∞ (MPa)	b	R_∞ (MPa)	b	R_∞ (MPa)
0.15%.	1.307	-56	4.005	-66	–	–
0.175%	1.197	-71	–	–	1.19	-76
0.2%	3.145	-80	4.169	-84	5.617	-80
0.25%	–	–	–	–	2.915	-81
0.3%	3.620	-84	1.734	-77	7.393	-82
0.35%	–	–	6.175	-77	–	–
0.4%	4.488	-83	5.099	-93	6.123	-76
0.5%	2.871	-52	5.426	-70	4.917	-64
0.6%	2.911	-52	–	–	–	–
0.7%	4.162	-69	1.484	-56	4.15	-81
Mean value	2.963	-68	4.015	-75	4.165	-77
Standard deviation	1.201	13.6	1.973	12.1	2.079	6.3
Confidence interval	1.958÷3.967	-79.7÷ -57.0	1.944÷6.085	-85.9÷ -63.5	2.693÷6.537	-83.0÷ -71.3
Value on merged data, b_{all} [a]	2.352	–	3.894	–	5.293	–

[a] Parameter b_{all} is estimated considering all data merged together as in Figure 11.

Table 5. Results of the analysis of variance on the elastic modulus and yield stress.

Parameter	*p*-value	*p*-value
	data at RT, 250 °C and 300 °C	data only at 250 °C, 300 °C
E_1	$3.6284 \cdot 10^{-09}$ (reject H_0)	0.09286 (accept H_0)
E_s	$3.4439 \cdot 10^{-09}$ (reject H_0)	0.98937 (accept H_0)
σ_{y0}	0.93062 (accept H_0)	0.86447 (accept H_0)
σ_{yc}	$4.9161 \cdot 10^{-07}$ (reject H_0)	0.86447 (accept H_0)

FIGURE CAPTIONS

Figure 1. (a) Specimen geometry; (b) Room temperature test: specimen clamped on the testing machine, with extensometer; (c) High-temperature test: water-cooled hydraulic grips, heating system (coil), and extensometer.

Figure 2. Stress-strain cycles (first and stabilised) recorded in tests at different temperatures, at strain amplitude ε_a=0.5%.

Figure 3. Sketch of combined kinematic and isotropic models in (a) in deviatoric stress space and (b) in uniaxial tensile loading.

Figure 4. Identification of yield stress: (a) initial yield stress σ_{y0} from the first one-quarter cycles; (b) cyclic yield stress σ_{yc} from the stabilised cycle.

Figure 5. Identification of cyclic yield stress σ_{yc} and plastic strain amplitude $\varepsilon_{pl,a}$ from experimental cycles at three different strain amplitudes at RT.

Figure 6. Experimental cyclic data at room temperature (markers) and fitted kinematic model (solid lines) for one, two or three pairs (C_i, γ_i) of kinematic variables.

Figure 7. Comparison between simulated and experimental stabilised cycles at RT, 250 °C, 300 °C, under the same strain range ε_a=0.5%. Simulations apply a kinematic model with one, two or three pairs (C_i, γ_i).

Figure 8. Comparison between simulated and experimental stabilised cycles at RT, under different strain amplitudes ε_a=0.3%, 0.4% and 0.6%.

Figure 9. Comparison between simulations and experiments: 5 cycles at RT and ε_a=0.5%. Simulations use the three-pair kinematic model with initial and stabilized values of E and σ_y.

Figure 10. Maximum stress vs. number of cycles, for tests at RT with different strain ranges applied.

Figure 11. Experimental cyclic data at room temperature (markers), fitted by the isotropic model in Eq. (10) (line).

Figure 12. Isotropic model fitted to room temperature data at strain amplitude: (a) ε_a=0.3% and (b) ε_a=0.5%.

Figure 13. Comparison between simulations and experiments: 80 cycles at RT and ε_a=0.5%. Simulations use a combined three-pair kinematic and isotropic model.

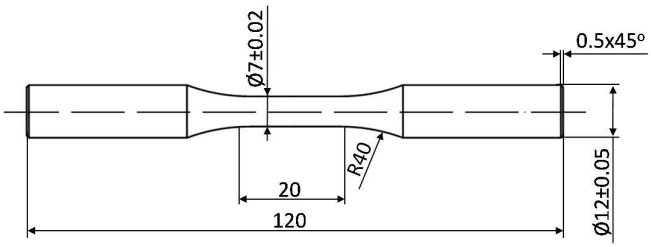

(a)

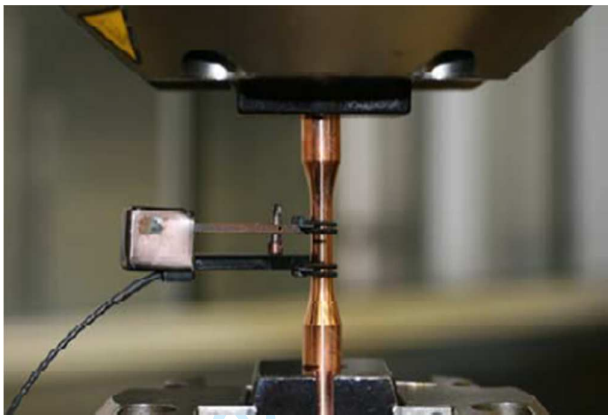

(b)

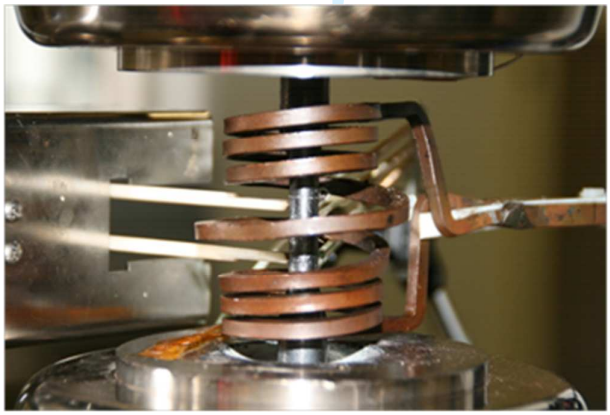

(c)

Figure 1. (a) Specimen geometry; (b) Room temperature test: specimen clamped on the testing machine, with extensometer; (c) High-temperature test: water-cooled hydraulic grips, heating system (coil) and extensometer.

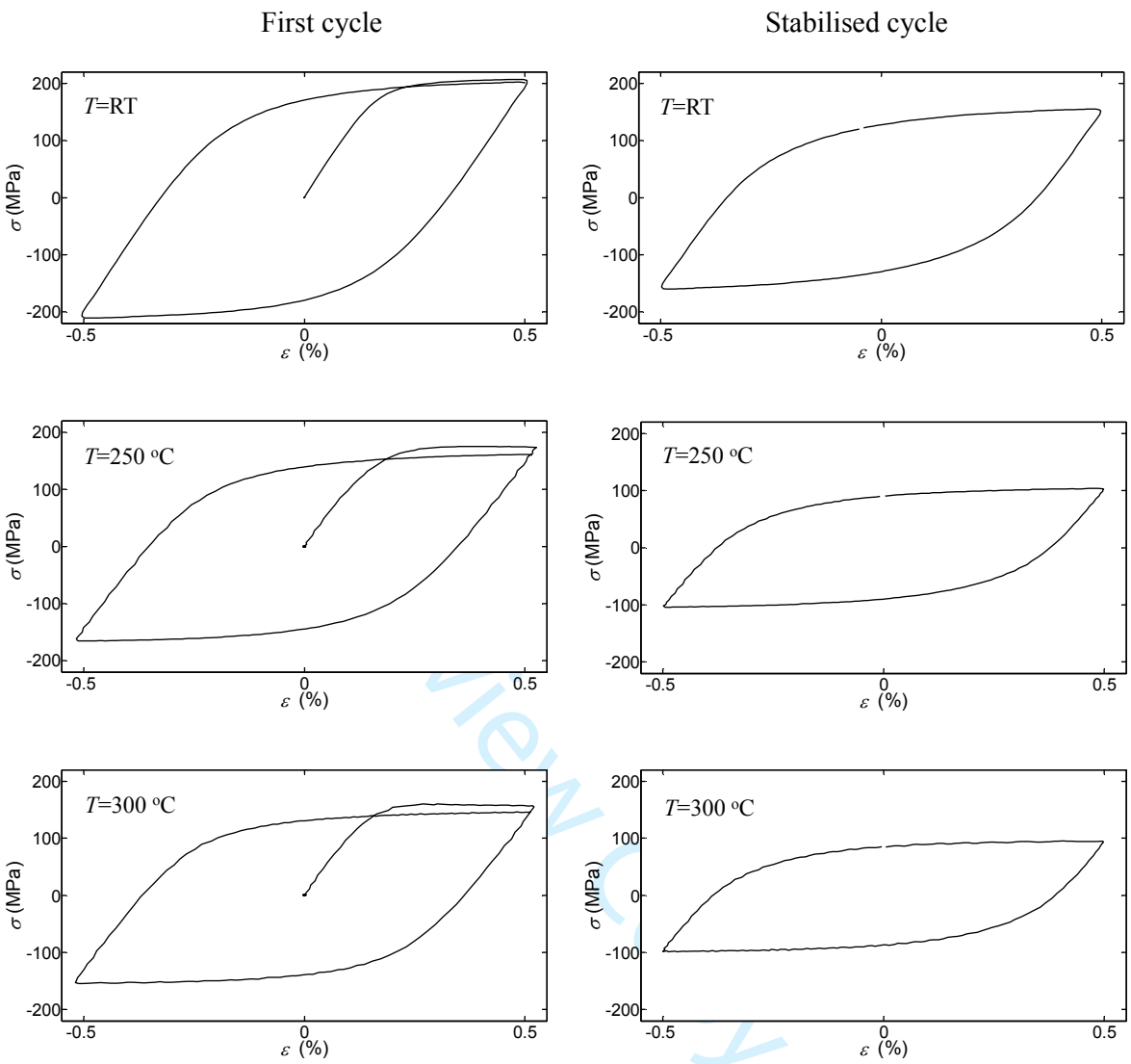

Figure 2. Stress-strain cycles (first and stabilised) recorded in tests at different temperatures, at strain amplitude ε_a=0.5%.

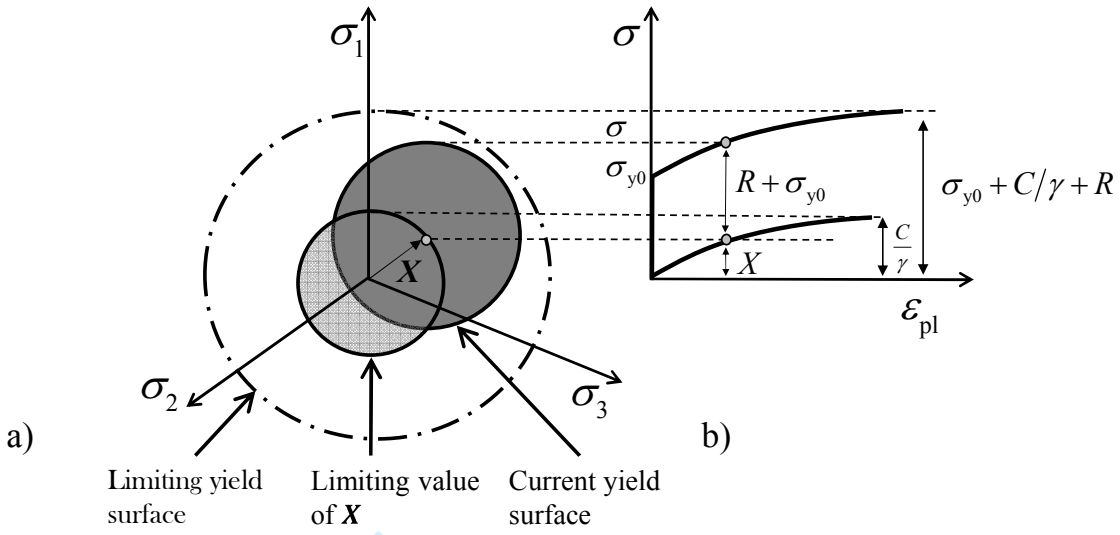

Figure 3. Sketch of combined kinematic and isotropic models in (a) in deviatoric stress space and (b) in uniaxial tensile loading.

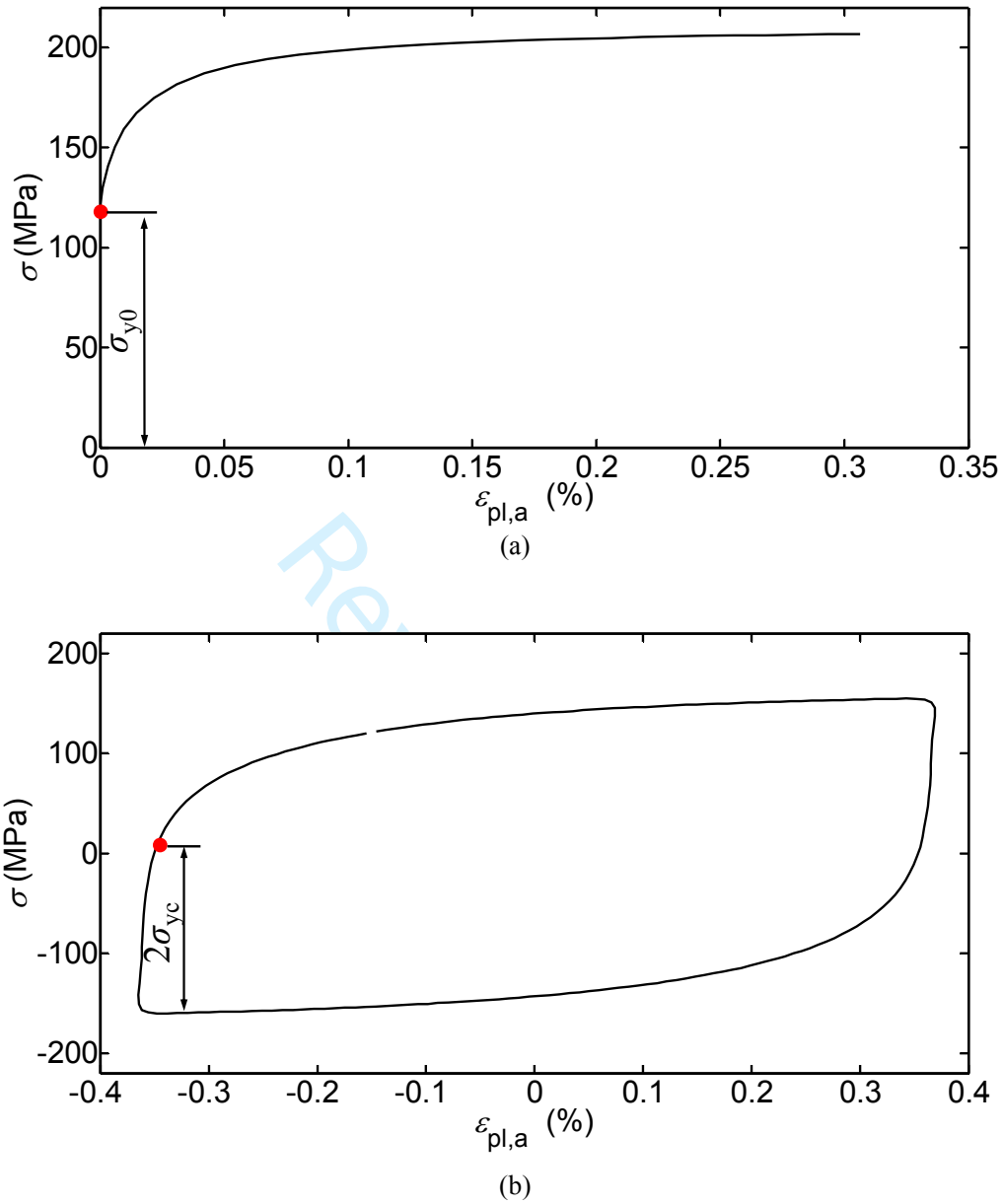

Figure 4. Identification of yield stress: (a) initial yield stress σ_{y0} from the first one-quarter cycles; (b) cyclic yield stress σ_{yc} from the stabilised cycle.

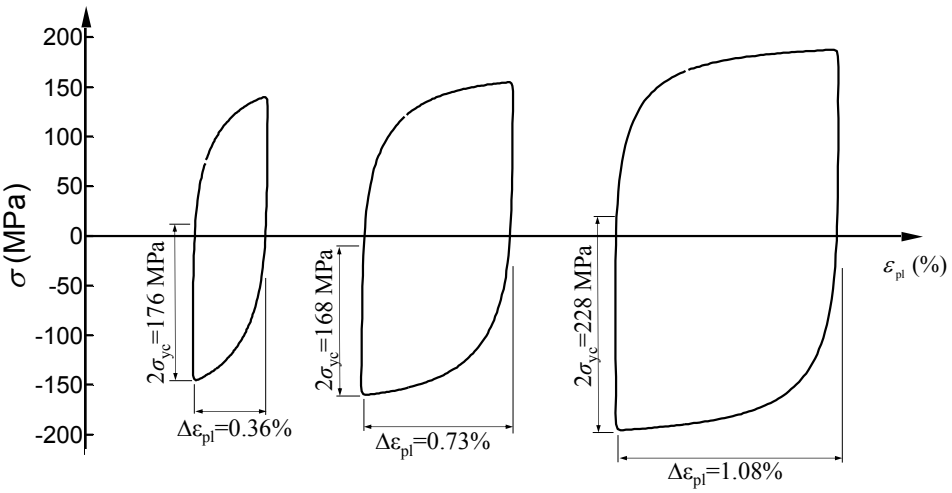

Figure 5. Identification of cyclic yield stress σ_{yc} and plastic strain amplitude $\varepsilon_{pl,a}$ from experimental cycles at three different strain amplitudes at RT.

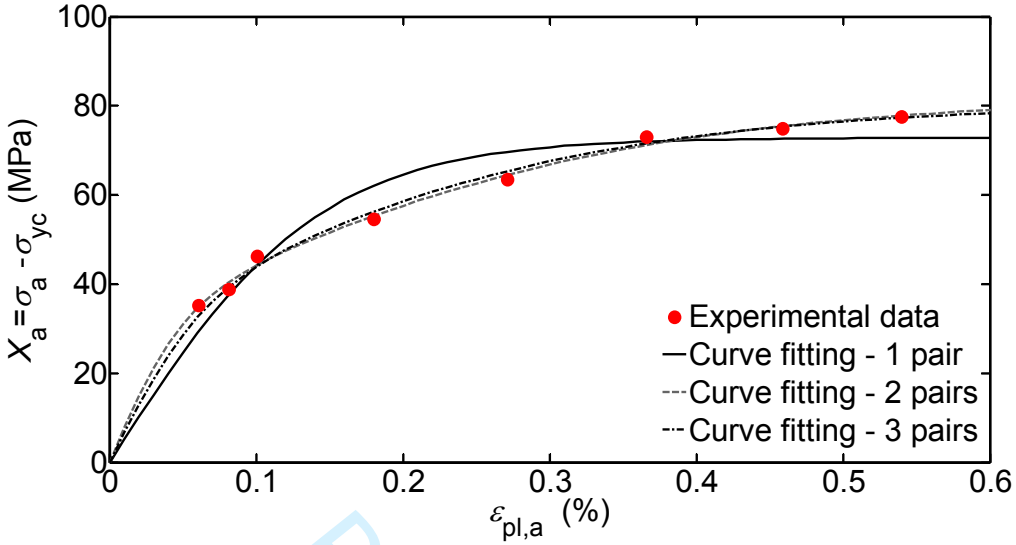

Figure 6. Experimental cyclic data at room temperature (markers) and fitted kinematic model (solid lines) for one, two or three pairs (C_i, γ_i) of kinematic variables.

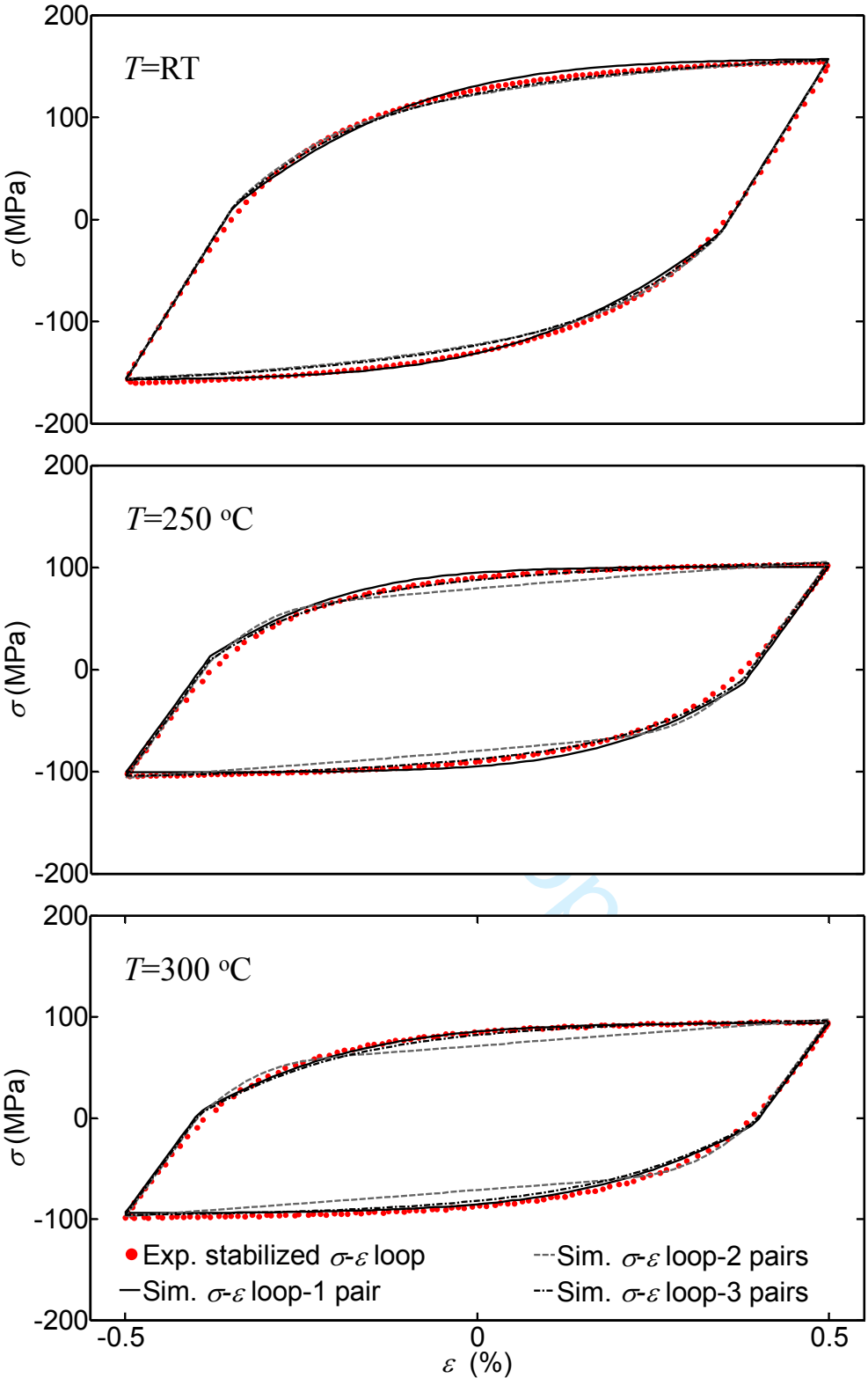

Figure 7. Comparison between simulated and experimental stabilised cycles at RT, 250 °C, 300 °C, under the same strain range ε_a=0.5%. Simulations apply a kinematic model with one, two or three pairs (C_i, γ_i).

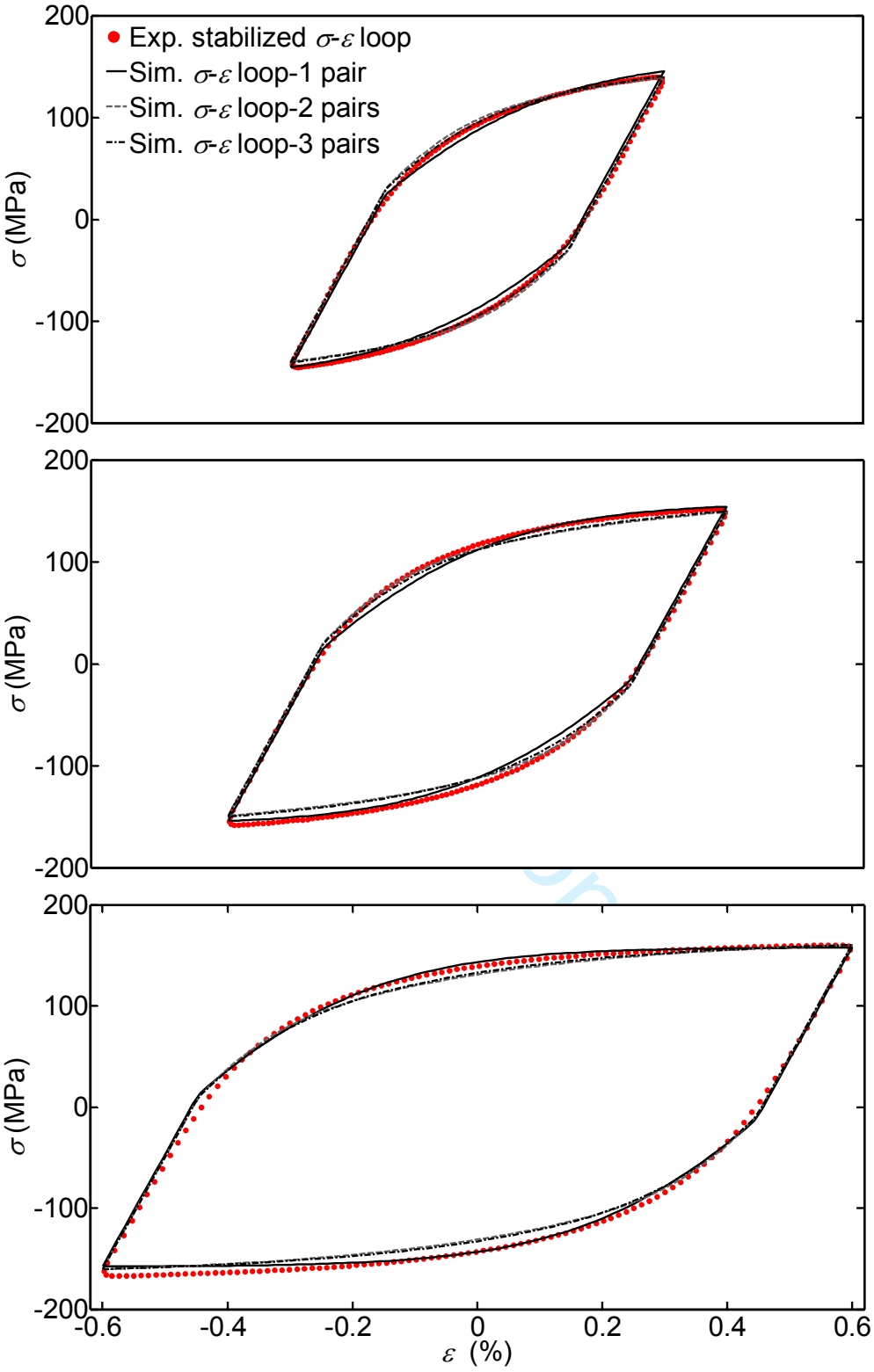

Figure 8. Comparison between simulated and experimental stabilised cycles at RT, under different strain amplitudes ε_a=0.3%, 0.4% and 0.6%.

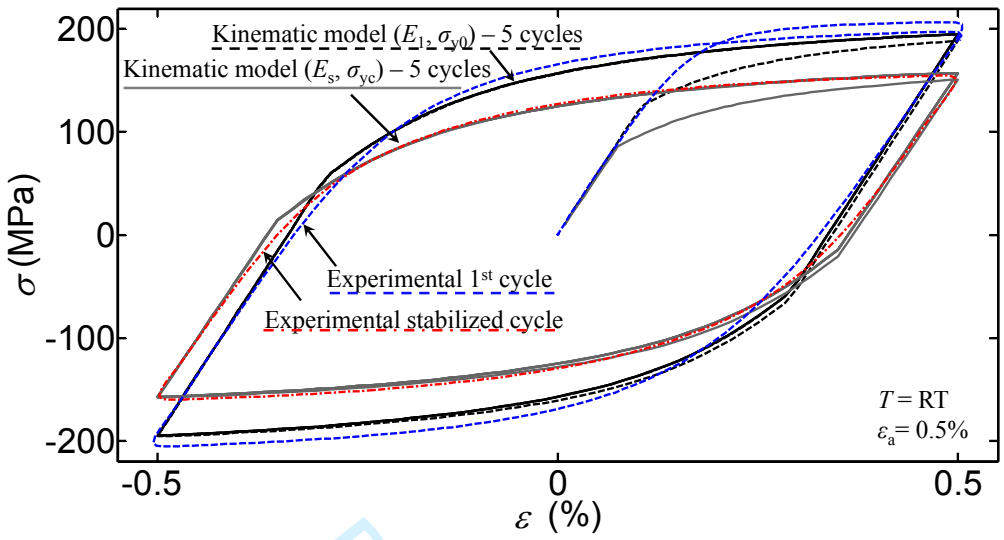

Figure 9. Comparison between simulations and experiments: 5 cycles at room temperature and ε_a=0.5%. Simulations use the three-pair kinematic model with initial and stabilized values of E and σ_y.

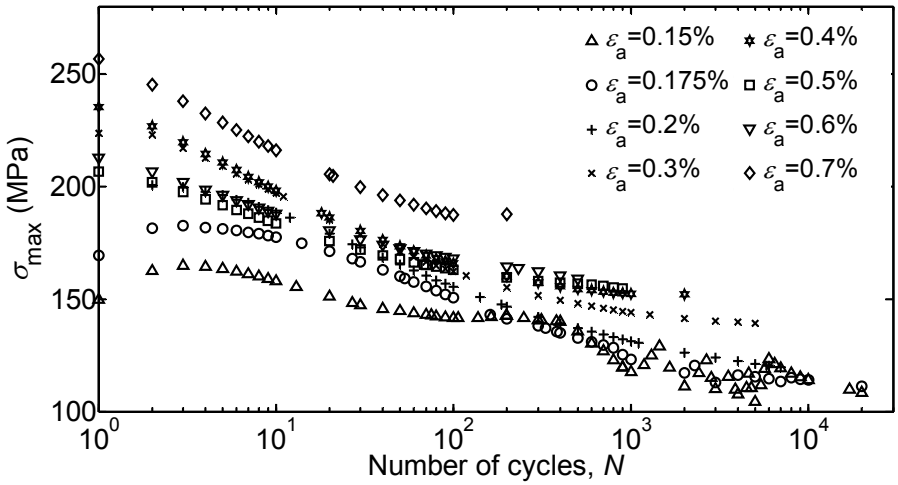

Figure 10. Maximum stress vs. number of cycles, for tests at RT with different applied strain ranges.

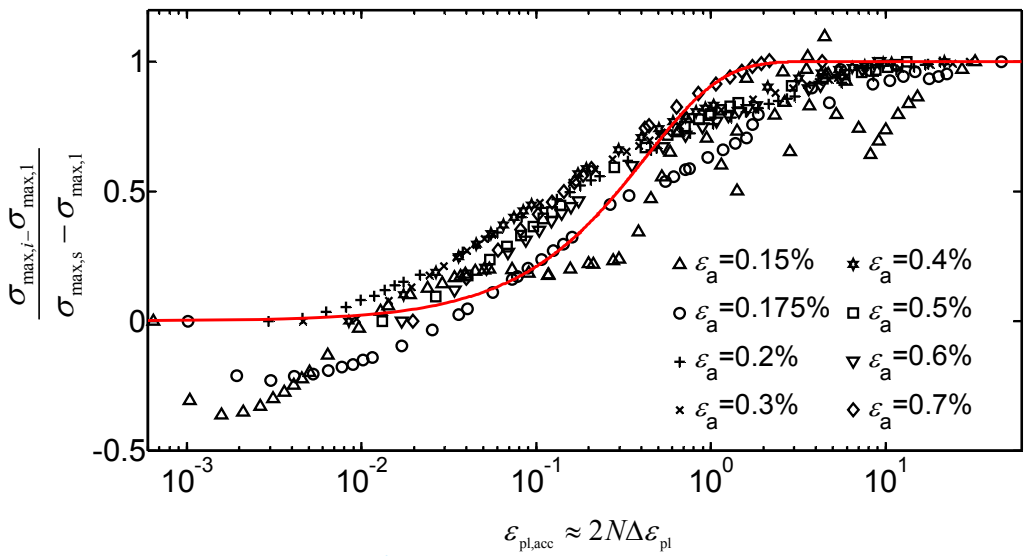

Figure 11. Experimental cyclic data at room temperature (markers), fitted by the isotropic model in Eq. (10) (line).

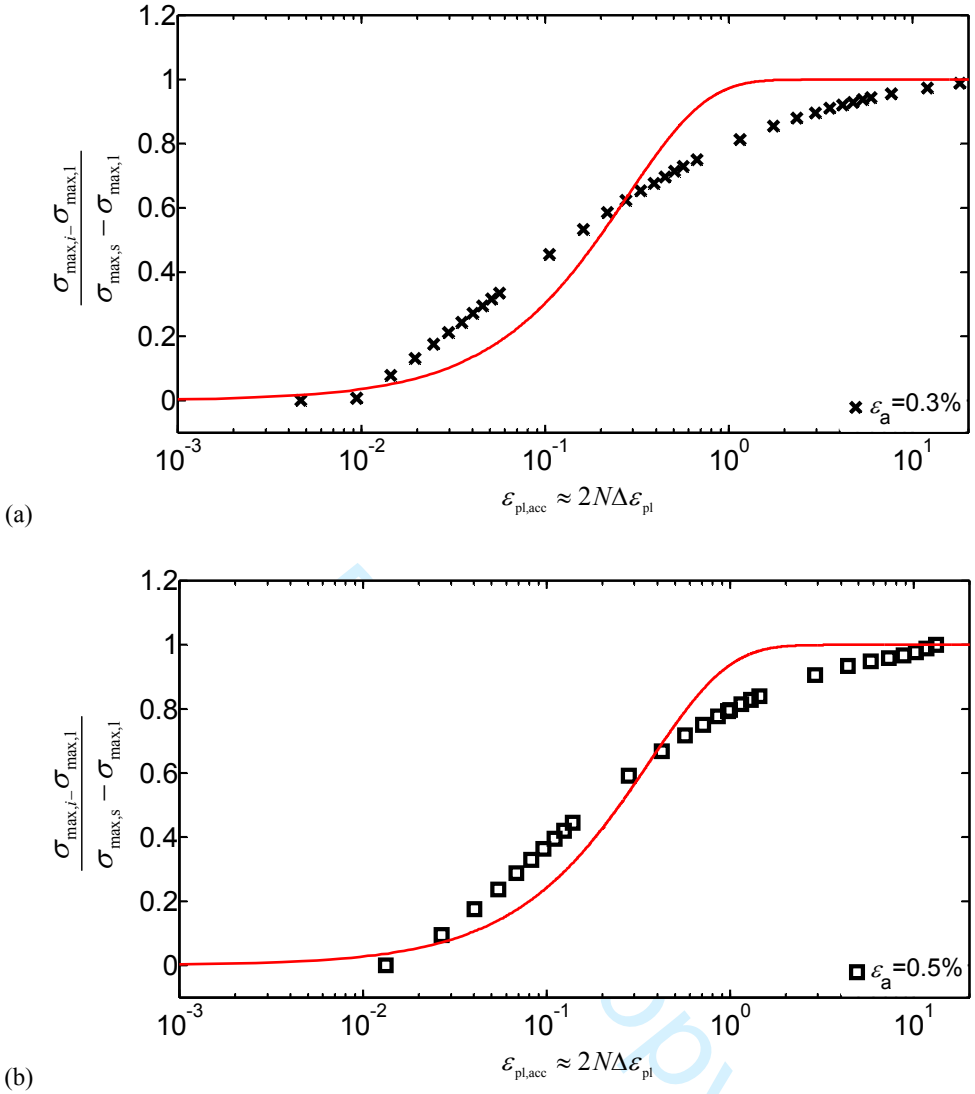

Figure 12. Isotropic model fitted to room temperature data at strain amplitude: (a) ε_a=0.3% and (b) ε_a=0.5%.

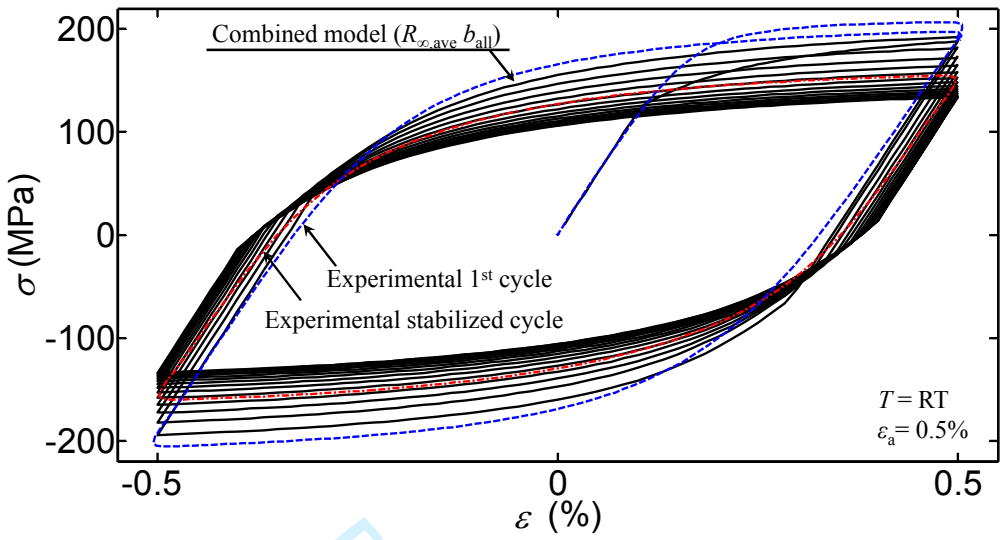

Figure 13. Comparison between simulations and experiments: 80 cycles at room temperature and ε_a=0.5%. Simulations use a combined three-pair kinematic and isotropic model.